Fachtagung „Lasermethoden in der Strömungsmesstechnik“
5.-7. September 2023, München

Planar seeding free measurement of time-averaged 2D3C velocity, pressure and temperature fields using the Filtered Rayleigh Scattering method

Planare seeding-freie Messung der zeitgemittelten 2D3C Geschwindigkeits-, Druck- und Temperaturverteilung mittels des Filtered Rayleigh Scattering Verfahrens

Michael Dues[1], Jonas Steinbock[1], Ulrich Doll[2], Ingo Röhle[3], Sergey Melnikov[3], Pavlos Zachos[4], Matteo Migliorini[4]

1) ILA R&D GmbH, Jülich, Germany
2) Paul Scherrer Institut (PSI), Villingen, Switzerland
3) Berliner Hochschule für Technik (BHT), Berlin, Germany
4) Cranfield University (CU), Cranfield, United Kingdom

Schlagworte: FRS, Partikelfrei, Messunsicherheit, Bildleiter
Key words: FRS, Seeding free, measurement uncertainty, Fiber Optic

Abstract

A Filtered Rayleigh Scattering (FRS) method is developed and applied to a ducted flow to obtain planar measurements of the pressure, temperature and velocity distribution without seeding. The region of interest is observed through an image fiber bundle which enables the simultaneous capture of six observation perspectives through one camera. The achieved spatial resolution is in the order of 1 mm^2.

To evaluate the performance of the method a laboratory scale test rig in DN 80 is build up and its flow field characterized with Laser Doppler Velocimetry (LDV). The deviation of the axial velocity component is less then 1 % in comparison with the LDV Reference. The static flow structures as well as the back flow region behind a swirl generator were obtained. Furthermore local temperature and pressure variations down to 5K resp. 10 hPa could be resolved.

Introduction

In the development of novel aircraft concepts, the reduction of fuel consumption and emissions is an important aspect. In this context, new concepts are being developed that integrate the engines into the aircraft body (Kim et al. (2013)). This causes, e.g. due to boundary layer flows, disturbed steady-state and transient inflows to the engines, which significantly affect their aerodynamic load and operational behavior (Doll et al. (2022)). To investigate such inflow disturbances, velocity and pressure distributions have so far often been recorded with grids of total pressure probes (SAE International (2017)), which, however, are limited in their ability to resolve the flow structures that occur in terms of their spatial and temporal resolution and are not without impact on the flow itself. For this reason, there is a need for measurement methods that are as non intrusive as possible and allow simultaneous detection of velocity, pressure and temperature fields in engine intakes. In order to be able to perform such inlet disturbance investigations not only in test bench tests but also potentially in flight tests, a measurement method that does not require the addition of seeding to the flow would be of great advantage. In the EU research project SINATRA “Seeding free non intrusive aero engine distortion measurements”, the possibility of using the Filtered Rayleigh

GALA e.V., Karlsruhe, Germany, ISBN 978-3-9816764-9-5

Scattering technique (FRS) for seeding-free investigation of inlet flows in engines on the test bench and potentially in flight tests is therefore being investigated. To this end, FRS measurements are first performed on a simplified flow experiment in order to optimize the experimental setup, characterize the measurement system and determine the measurement uncertainty. In a second step, FRS measurements of the pressure and velocity field are then carried out on a test rig for the investigation of engine intakes at Cranfield University. This paper presents the setup of the measurement system, the simplified test rig, and initial measurement results.

The outline of this paper is as follows: After describing the measurement principle, the main system components, as well as characterizing the test section, preliminary investigations are presented to validate the method on a conditioned pipe flow in comparison to laser Doppler velocimetry (LDV) measurements. This is followed by the application of the FRS method to a swirling flow.

Test rig

The simplified experimental setup (Figure 1) consists of a conditioned pipe flow with an inner Diameter d_i=80 mm. In this measuring cross-section flow velocities of approx. 30 to 100 m/s can be generated. Optical access is provided by an anti-reflective-coated glass tube. The laser light sheet is coupled in via a slit in the glass tube.

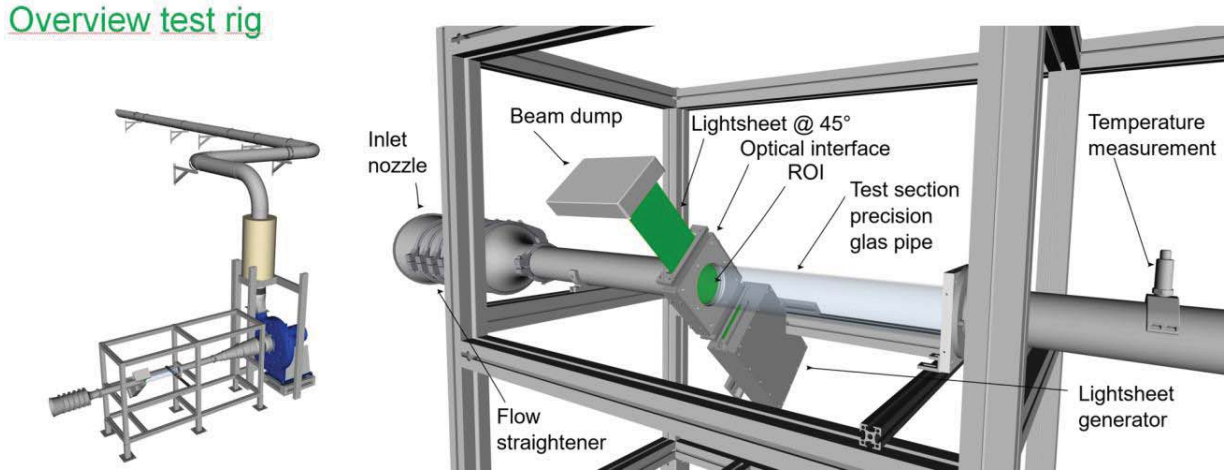

Figure 1: Test rig for the investigation of pipe flows

Due to the flow straightener, the contraction of the flow in the inlet nozzle and the relatively short distance to the measurement cross-section, a fully developed pipe flow profile is not expected. For subsequent validation of the FRS measurements, the axial velocity field in the pipe is recorded for three operating points using LDV. For this purpose, the local axial velocity is determined by traversing the LDV probe on a measuring grid with 305 measuring points. Figure 2 shows the measured velocity distribution for the three operating points.

GALA e.V., Karlsruhe, Germany, ISBN 978-3-9816764-9-5

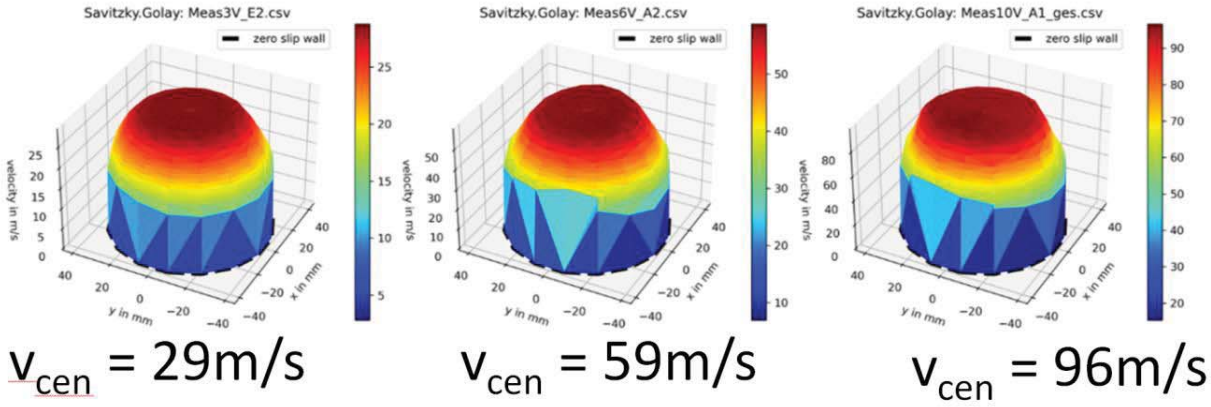

Figure 2: Representation of the axial velocity over the measuring cross-section for three volume flows at 30%, 60% and 100% of the test rig. The dashed line corresponds to the zero-slip wall condition.

Due to the relatively short pipe length (6D) between the inlet nozzle and the measuring cross-section, a developing turbulent pipe flow profile is formed there, characterized by a top-hat distribution in the center of the pipe, which drops off with a strong gradient towards the wall in the peripheral area of the flow. By integrating the velocity profile over the measuring cross-section, the volumetric flow and the mean volumetric velocity can be calculated.

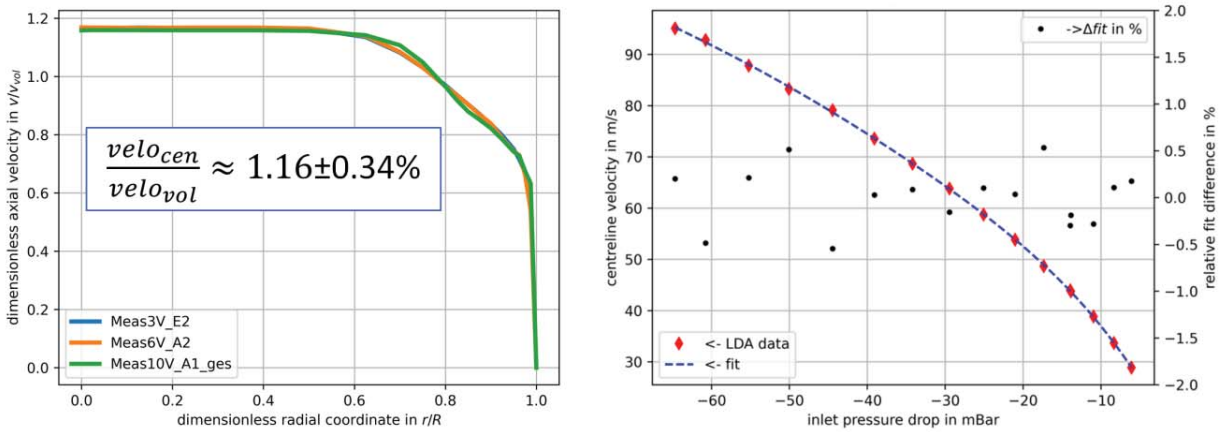

Figure 3: (left) Plot of dimensionless axial velocity versus dimensionless radius. The ratio between centerline velocity and volumetric velocity is 1.16 +/- 0.34%. (right) Centerline velocity plotted versus pressure drop at the inlet nozzle (red diamonds). The dashed blue line is a polynomial to approximate the measured values. The black circles describe the relative deviation of the fit to the measured values.

Figure 3 (left) shows that the velocity distributions normalized to the volumetric velocity are almost congruent for all operating points and thus the shape of the velocity profiles does not change. Therefore, the volumetric flow can also be determined by measuring the centerline velocity (single-point measurement).

The centerline velocity as well as the pressure drop at the inlet nozzle is subsequently determined over the fan operating range of 30%-100% for 15 volume flows (Figure 3, right). Thus, for subsequent FRS measurements, when the nozzle pressure is measured, both the volume flow,

GALA e.V., Karlsruhe, Germany, ISBN 978-3-9816764-9-5

the mean velocity and the normalized velocity profile are known. The volumetric flow can thus be adjusted solely by the pressure drop of the nozzle.

FSM-FRS measuring principle

The FRS method is based on the evaluation of the Rayleigh scattering of laser light from gas molecules in the flow. The Rayleigh scattering from gas molecules has a spectral width of several GHz and contains information about temperature, pressure, velocity and density in the illuminated measurement area. Strong reflections of laser light from walls (geometric scattering) or from particles (Mie scattering) are not broadened in frequency and can be effectively filtered out of the measurement signal with the aid of a molecular filter, in this case an iodine cell.

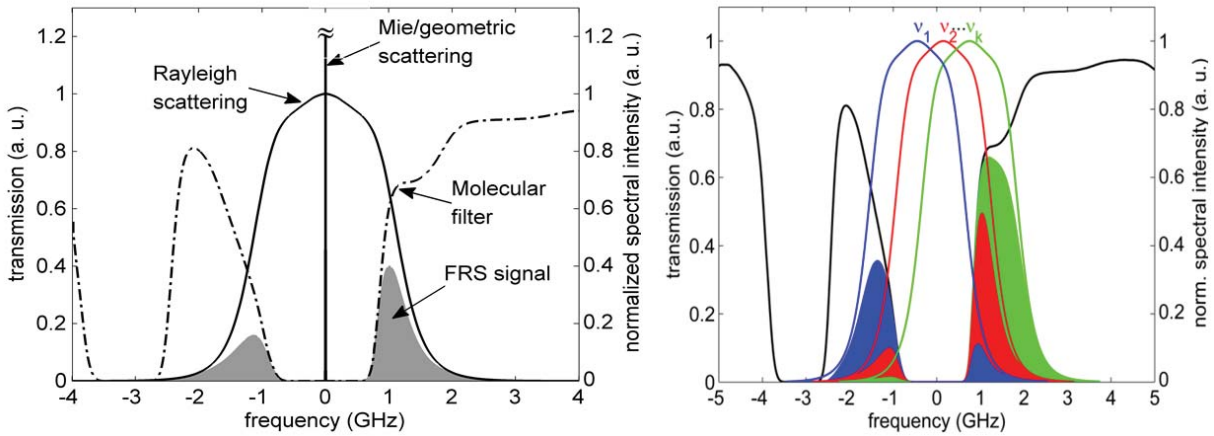

Figure 4: (left) Rayleigh-scattered light from the narrowband laser is filtered by an iodine cell, which removes reflections from surfaces and scattering from large particles (Mie scattering). (right) Frequency scan method: the laser frequency is shifted along the transmission profile of the molecular filter. From the resulting intensity spectra, time-averaged pressure, temperature and velocity fields (Doppler shift) can be determined simultaneously

The light scattered by the molecules is imaged through the iodine cell onto a CCD sensor and transformed into an intensity value. However, this results in the loss of spectral information about temperature, pressure, density and velocity. According to the frequency scan FRS method (FSM-FRS) further developed by DLR Cologne, the frequency of the laser system is therefore varied in discrete steps along the filter curve of the iodine cell, so that an intensity curve dependent on the laser frequency is produced for each pixel (Doll et al. (2014)). From this intensity curve, the temperature, pressure, velocity and density can be reconstructed using a suitable measurement model (Dues et al. (2018)).

The measuring system

The FRS system consists of a frequency-controlled laser, a wavelength meter, a light arm, a light sheet generator, a multi-arm image fiber bundle with lenses, a camera module with iodine cell and a CMOS camera. The laser used is a fiber laser from the manufacturer Azurlight Systems (5W, 532.3 nm) in conjunction with an NKT seed laser. The laser is characterized by a relatively small spectral width of less than 200 kHz and a wide frequency adjustment range.

GALA e.V., Karlsruhe, Germany, ISBN 978-3-9816764-9-5

To scan along the selected iodine absorption line, the frequency of the fiber laser is shifted in the range of 8 GHz. The wavelength of the fiber laser is detected with the wavelength meter compared to a stabilized HeNe laser and controlled with a control output to the fiber laser (Figure 5, (a)).

The light sheet probe is equipped with a rotating prism that moves the laser beam across a line. This allows a uniform intensity distribution to be realized across the width of the light sheet. A PCO Edge 4.2 CMOS camera is used as the detector at an exposure time of 20 s per frequency step. To allow the simultaneous determination of three velocity components, the pressure and the static temperature, the measurement cross-section is viewed from six perspectives through a 6-arm image fiber bundle with about 50000 fibers per arm and imaged onto the sensor of the camera.

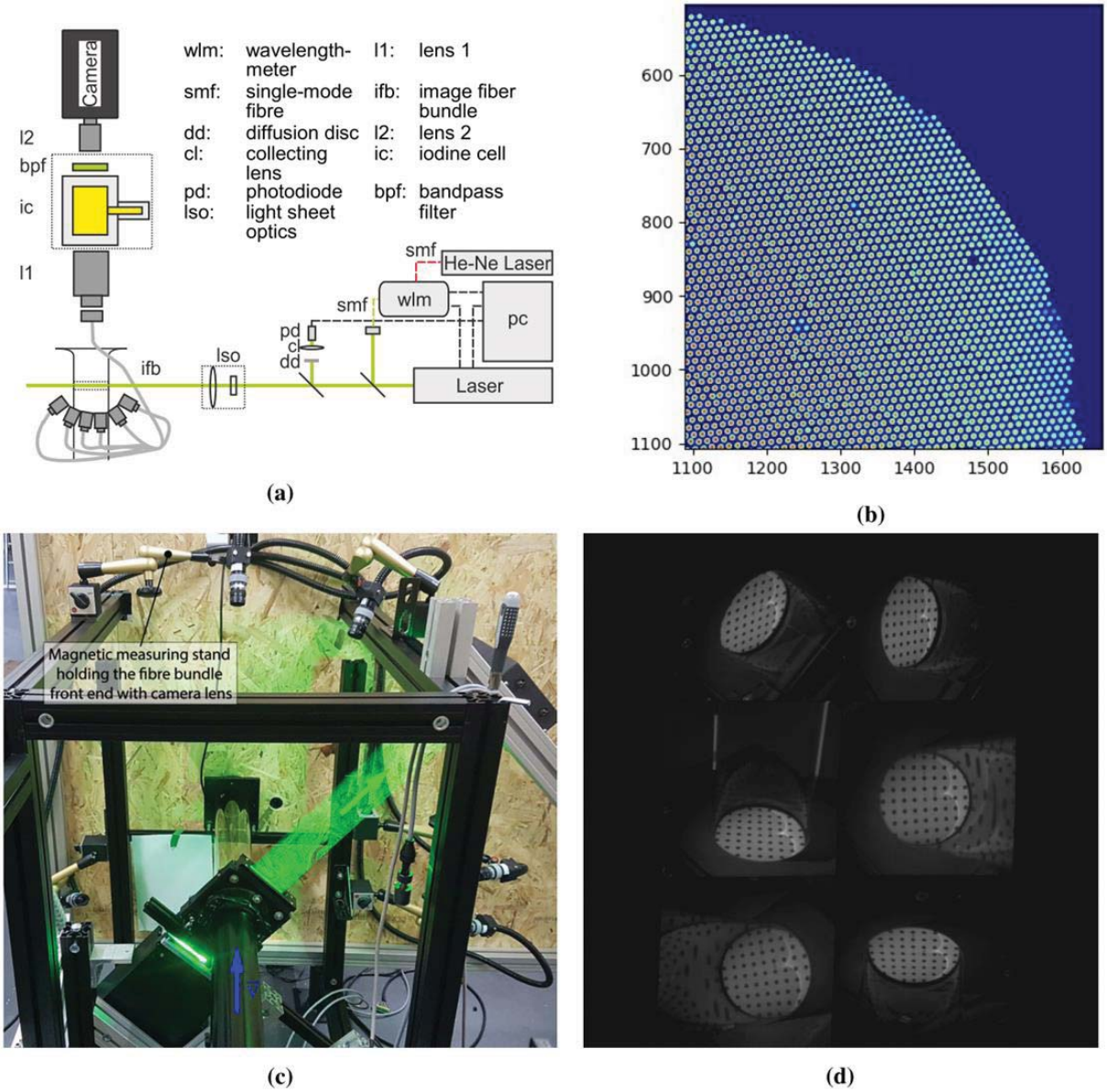

Figure 5: (a) Components of the FRS measurement system, (b) Detail view Image fiber, (c) Arrangement of the six observation perspectives, (d) The six views of the calibration target on the camera chip.

GALA e.V., Karlsruhe, Germany, ISBN 978-3-9816764-9-5

Evaluation

First, the position of each camera perspective in relation to the coordinate system of the measurement cross-section is determined. For this purpose, a calibration image (target) is introduced into the measurement cross-section. The calibration image consists of planar circles with a known (grid) size. The circles are then automatically detected on the camera image. To assign the known spatial coordinates, a regular grid is placed over the respective target image. By moving the vertices, the grid is transformed linearly and can be adapted to the recognized grid points. Using a previous camera calibration based on Python's OpenCV toolbox, the respective image rectification is calculated from the mappings detected in this way and the camera position is determined. From the camera position, the individual observation vector is determined for each pixel in the measurement cross-section.

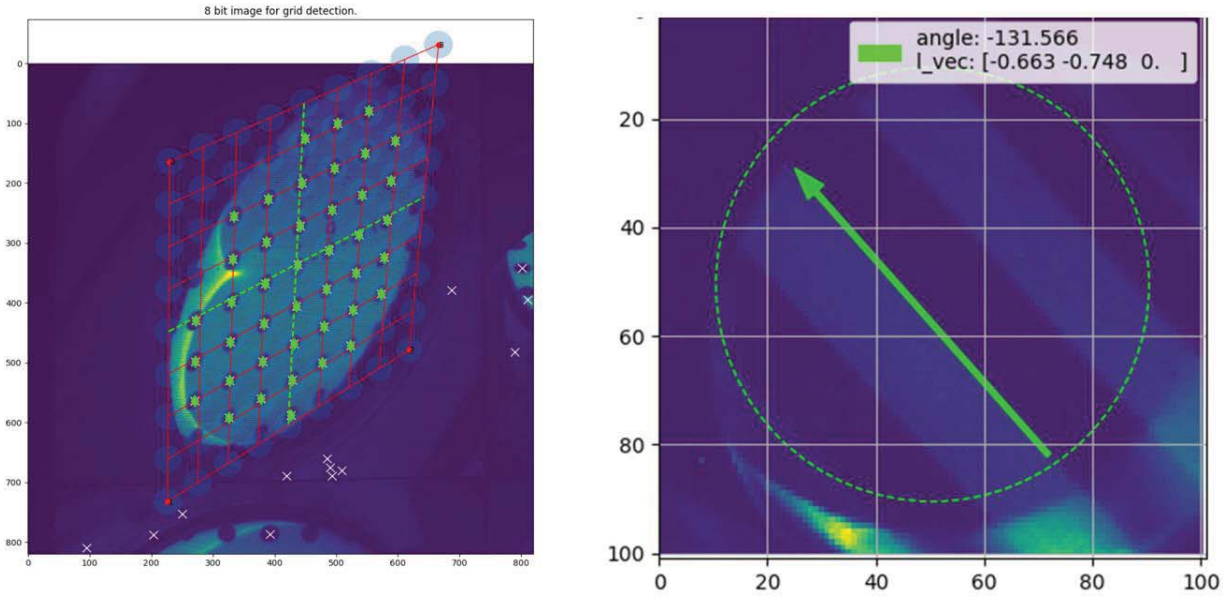

Figure 6: (left) Semi-automatic detection and assignment of points on the calibration image to determine the camera perspective. Detected target points are depicted as white x, the movable grid is displayed in red lines, the local search region is displayed as transparent circle and the valid points are depicted by greed diamonds. (right) Determination of the laser vector for camera 1.

Furthermore, the direction vector of the laser beam in the measuring plane is determined. For this purpose, a stripe pattern in the laser sheet plane is formed by using an aperture with regular slits. After rectification of the image according to the previous description, a straight line is fitted to an edge of the laser stripe. This straight line corresponds to the direction vector of the laser light (Figure 6, right).

The camera calibration, image rectification and geometry calculations are performed using the OpenCV (Bradski (2000)) library.

For the evaluation of the measurements, a spectral model of the Rayleigh scattering is convoluted with the calibrated transmission spectrum of the iodine cell, and then fitted to the measured intensity(s) with a least square calculation. The evaluation is performed for each pixel in the rectified measurement grid.

GALA e.V., Karlsruhe, Germany, ISBN 978-3-9816764-9-5

Each pixel in the computational domain corresponds to a resolution of 1 mm^2 in the measurement plane. First, several experimental parameters are calibrated using a reference measurement. For this purpose, a measurement is made without flow (u=v=w=0) and at known pressure and temperature. For each pixel a local compensation calculation is then performed to determine a background parameter (c_t) as well as a scaling parameter (optical efficiency). This is done separately for all 6 perspectives.

After calibration, the actual measurements can be evaluated. For this purpose, the flow parameters p, T, u, v, w are fitted with a least square calculation (Levenberg-Marquardt) using the previously determined calibration parameters.

Different models for Rayleigh scattering are implemented in the calculation software. The reference model is the Tenti-S6 model, which is computationally expensive. Further implemented is a calibrated model developed by DLR (Doll et al. (2016)), as well as a newer, efficient approximation of the Tenti model based on a machine learning approach. Another ML implementation, which takes into account not only the Rayleigh spectrum but also the transmission curve of the iodine cell, is currently being developed by BHT.

A detailed description of the systematics for evaluation is presented in Doll (Doll et al. (2023)) and Doll et al. (Doll et al. (2017)).

Results

Figure 7 shows radially averaged velocity profiles (a) measured with FRS for three operating points in comparison to the velocity profiles measured with LDV ([4]). In the center region of the flow, the flow profile is strongly flattened in both the LDV and FRS measurements, while closer to the walls a flow gradient occurs due to the boundary layers building up. In the center region, the difference between FRS and LDV measurement is less than 1%. In the region close to the wall, the velocity of the LDV measurement drops more sharply, but this can be explained by the measurement position of the LDV measurement further downstream. The static pressure (a) measured by FRS agrees very well with the integral reference pressure measured behind the nozzle. The same is true for the FRS based temperature (b) compared to the isentropic calculated reference temperature in the flow cross section.

GALA e.V., Karlsruhe, Germany, ISBN 978-3-9816764-9-5

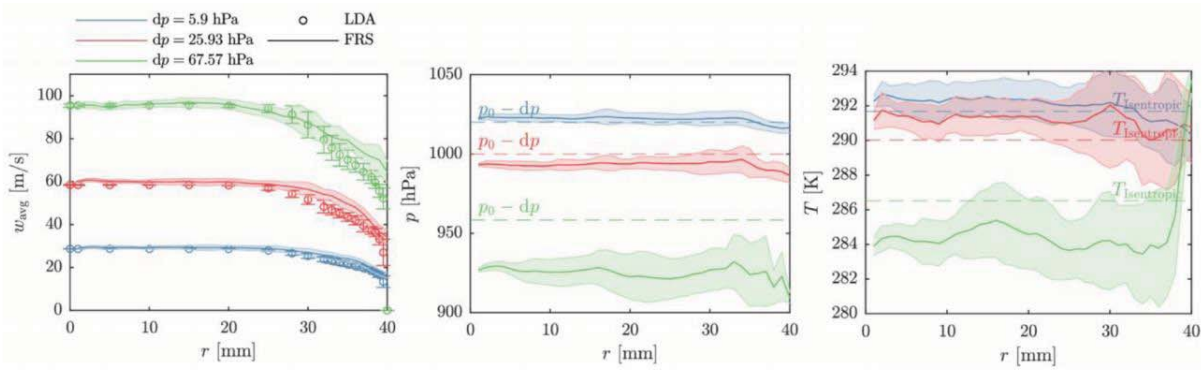

Figure 7: (a) Comparison of the axial velocity profiles measured with LDV and FRS, (b) Comparison of the distribution of static pressure (a) and static temperature (c) measured with FRS with the integral comparison values of the test rig.

In the next step, measurements were made behind a swirl generator (Figure 8), which was first installed 0.25 D and then approx. 7 D upstream of the measurement cross section.

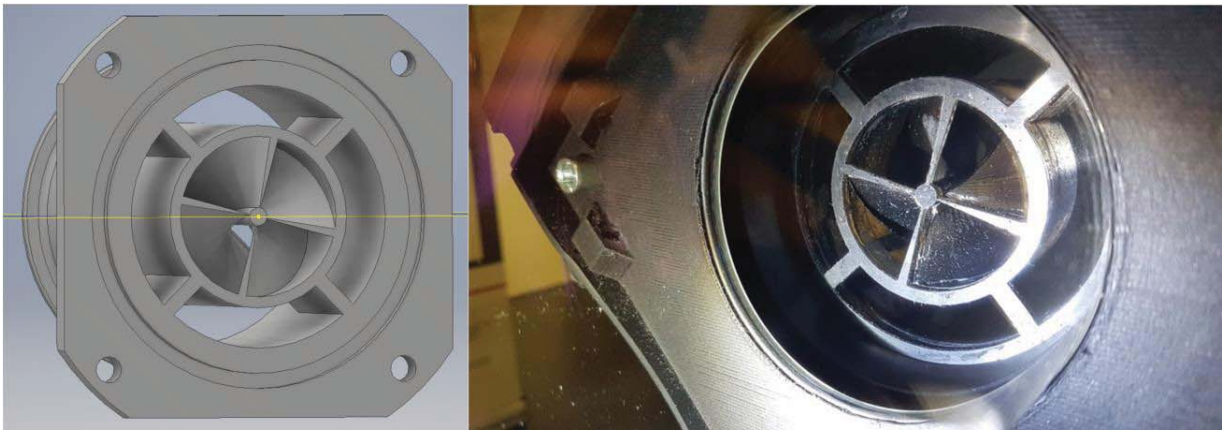

Figure 8: Swirl generator with four channels for installation in the test bench

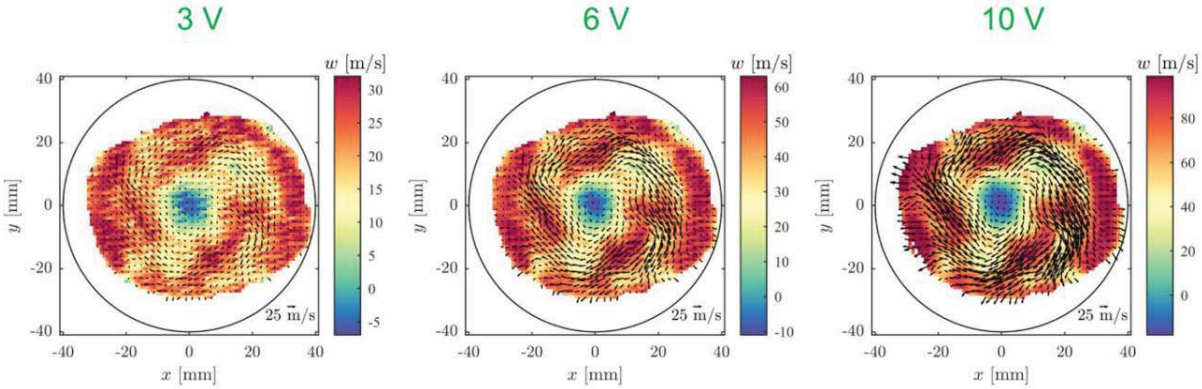

Figure 9: Velocity distribution 20mm behind the swirl generator at three different operating points

GALA e.V., Karlsruhe, Germany, ISBN 978-3-9816764-9-5

In the next step, measurements were made behind a swirl generator. Figure 9 shows the measured 3C velocity distribution approximately 20 mm behind the swirl generator for the three operating points 30m/s (3V), 60 m/s (6V) and 100m/s (10V). For all operating points, the circumferential components of the velocity in the secondary flow are clearly visible. Even the wake dents of the four swirl vanes are well identified, especially in the distribution of the axial component w. In the center of the flow field, a backflow region is evident.

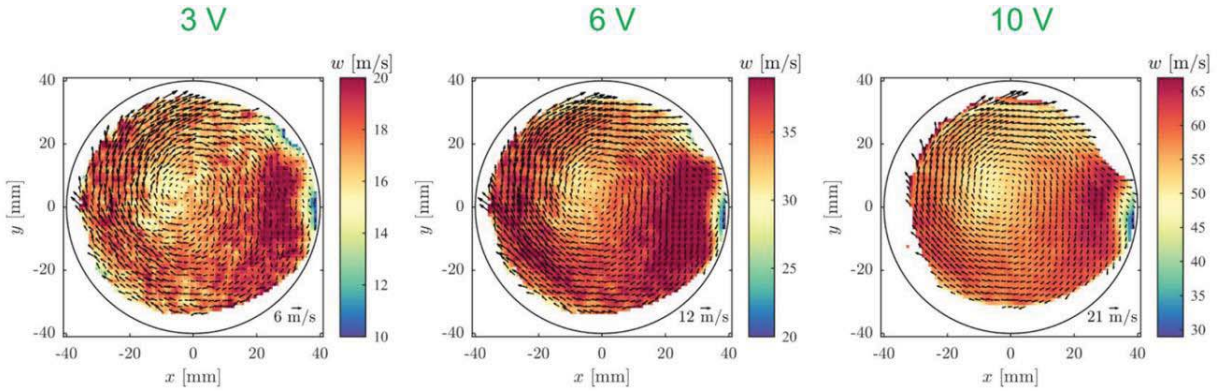

Figure 10: Velocity distribution 7D behind the swirl generator at three different operating points

The FRS measurement about 7D behind the swirl generator shows, as expected, a considerable homogenization of the flow field with a slight displacement of the vortex center (Figure 10).

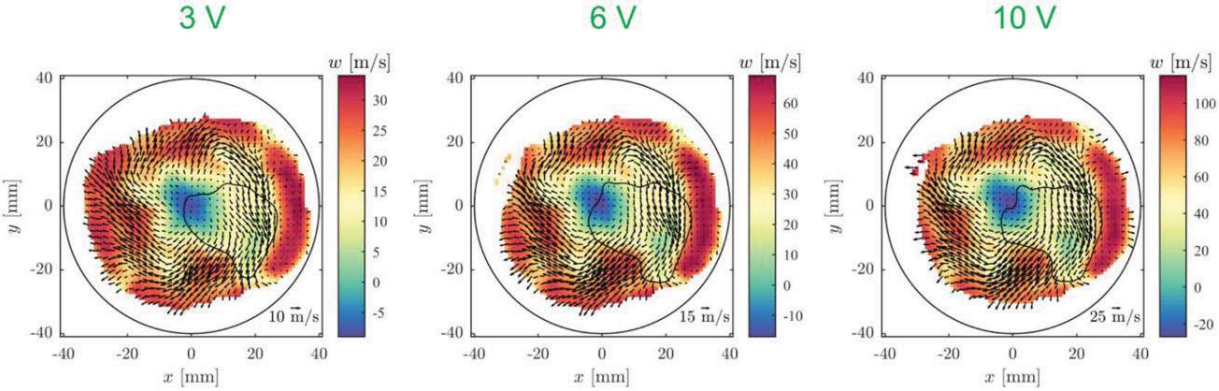

Figure 11: Velocity distribution 20 mm downstream of the swirl generator with warm air blown in one channel

To test the FRS temperature measurement, hot air with comparatively low velocity was fed through a glass tube into one of the swirler's passages. Compared to the corresponding results in Figure 9, a lower velocity region is clearly visible in the axial velocity component w in a partial segment behind the swirl generator (Figure 11).The contour drawn corresponds to the zone of increased temperature due to the hot gas injection in Figure 12.

GALA e.V., Karlsruhe, Germany, ISBN 978-3-9816764-9-5

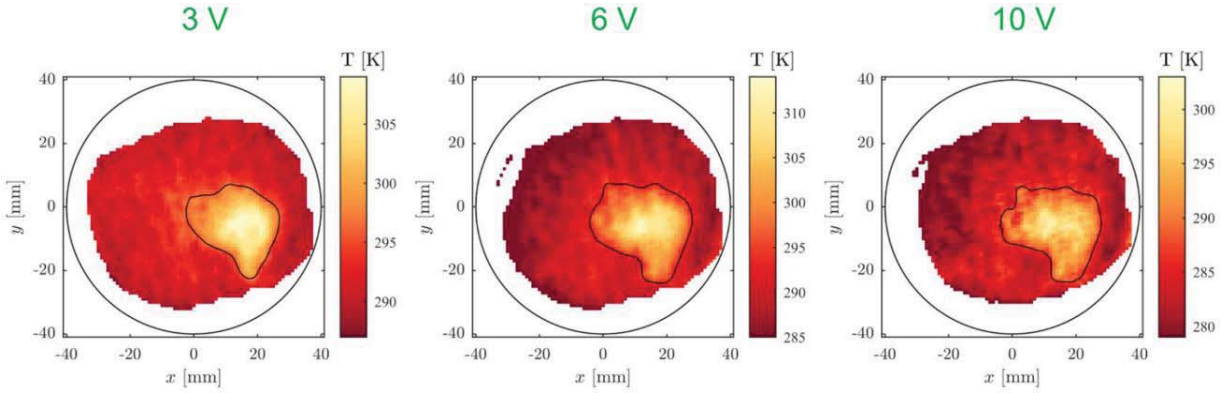

Figure 12: Temperature distribution 20 mm downstream of the swirl generator with hot air blown in one channel

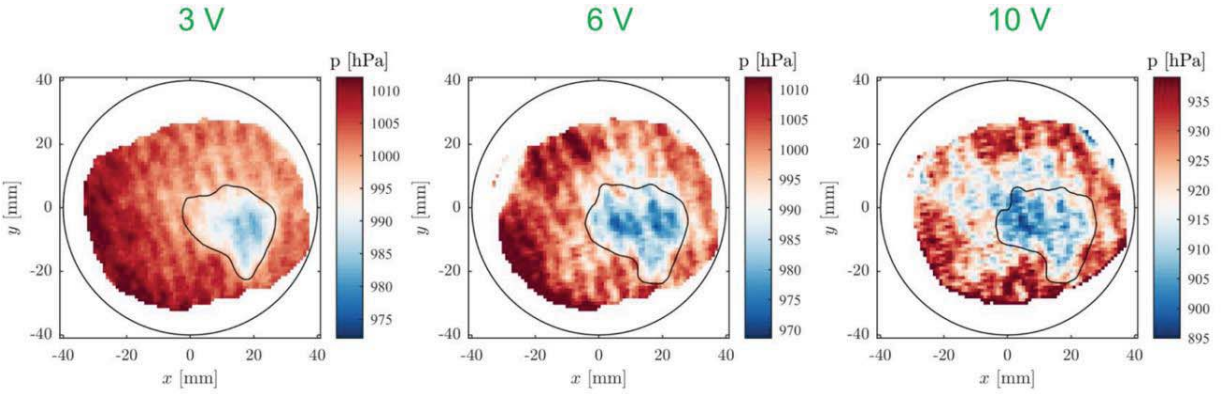

Figure 13: Static pressure distribution 20 mm behind the swirl generator with warm air blown in one channel

The additional flow resistance due to the inserted glass tube leads to a reduction of the static pressure in this area(Figure 13).

Summary and outlook

The measurements presented here show that 2D3C velocity measurements as well as the simultaneous acquisition of temperature and pressure fields with the FRS technique in a DN80 pipe flow is possible without the addition of seeding. With undisturbed inflow, the deviations in the axial velocity component are less than 1% compared to LDV measurements. The pressure and temperature values determined by FRS also agree well with the respective reference values. The FRS measurements in the downstream flow 20 mm behind a swirl generator show the expected strong swirl components as well as a backflow zone in the center of the measurement cross section. The wake areas of the swirl blades are also clearly visible. The preheated air separately supplied through a glass pipe can be clearly detected by the FRS temperature measurement and is also visible in the associated pressure field. The next step will be to test the method on a test rig at Cranfield University, which has been specially developed for investigating inlet flow distortions relevant to aero-engines.

GALA e.V., Karlsruhe, Germany, ISBN 978-3-9816764-9-5

Acknowledgements

This project has received funding from the Clean Sky 2 Joint Undertaking (JU) under grant agreement No 886521. The JU receives support from the European Union's Horizon 2020 research and innovation programme and the Clean Sky 2 JU members other than the Union.

Literature

Bradski, G. 2000. "The OpenCV Library." *Dr. Dobb's Journal of Software Tools*.

Doll, U., M. Beversdorff, G. Stockhausen, C. Willert, D. Schlüß, and C. Morsbach. 2014. "Characterization of the flow field inside a ranque-hilsch vortex tube using filtered rayleigh scattering, laser-2-focus velocimetry and numerical methods." *International Symposium on Applications of Laser Techniques to Fluid Mechanics*.

Doll, U., E. Burow, G. Stockhausen, and C. Willert. 2016. "Methods to improve pressure, temperature and velocity accuracies of filtered rayleigh scattering measurements in gaseous flows." *Measurement Science and Technology*, 27 (12): 125204. IOP Publishing. https://doi.org/10.1088/0957-0233/27/12/125204.

Doll, U., R. Kapulla, J. J. Steinbock, M. Dues, M. Migliorini, and P. K. Zachos. 2023. "Seeding-free inlet flow distortion measurement by filtered Rayleigh scattering: diagnostic approach and verification." *AIAA SciTech Forum*.

Doll, U., M. Migliorini, J. Baikie, P. K. Zachos, I. Röhle, S. Melnikov, J. Steinbock, M. Dues, R. Kapulla, D. G. MacManus, and N. J. Lawson. 2022. "Non-intrusive flow diagnostics for unsteady inlet flow distortion measurements in novel aircraft architectures." *Progress in Aerospace Sciences*, 130: 100810. Elsevier BV. https://doi.org/10.1016/j.paerosci.2022.100810.

Doll, U., G. Stockhausen, and C. Willert. 2017. "Pressure, temperature, and three-component velocity fields by filtered Rayleigh scattering velocimetry." *Optics Letters*, 42 (19): 3773. The Optical Society. https://doi.org/10.1364/ol.42.003773.

Dues, M., U. Doll, T. Bacci, A. Picchi, G. Stockhausen, and C. Willert. 2018. "Laseroptische Untersuchung des Strömungsfeldes hinter dem Turbinengitter eines Simulationsprüfstandes mittels Filtered Rayleigh Scattering." *Fachtagung "Experimentelle Strömungsmechanik"*.

Kim, H. D., J. L. Felder, Michael. T. Tong, and M. Armstrong. 2013. "Revolutionary aeropropulsion concept for sustainable aviation: Turboelectric distributed propulsion." *International Society for Air Breathing Engines ISABE--2013--1719*.

SAE International. 2017. "Gas turbine engine inlet flow distortion guidelines." *AEROSPACE Standard ARP 1420C*. SAE International. https://doi.org/10.4271/arp1420c.

GALA e.V., Karlsruhe, Germany, ISBN 978-3-9816764-9-5